IEEE Access
Multidisciplinary ⋮ Rapid Review ⋮ Open Access Journal

Received March 3, 2019, accepted March 14, 2019, date of publication March 19, 2019, date of current version April 8, 2019.

Digital Object Identifier 10.1109/ACCESS.2019.2906189

Complex Impedance Transformers Based on Allowed and Forbidden Regions

HEE-RAN AHN, (Senior Member, IEEE), AND MANOS M. TENTZERIS, (Fellow, IEEE)
School of Electrical and Computer Engineering, Georgia Institute of Technology, Atlanta, GA 30332, USA

Corresponding author: Hee-Ran Ahn (hranahn@gmail.com)

This work was supported in part by the NSF.

ABSTRACT Three mapping functions are for the first time derived for allowed and forbidden regions of a complex impedance transformer with only one transmission-line section (TL). The divided sections of the allowed and forbidden regions are six for transforming real into complex impedances, and those for both complex termination impedances are 14, indicating that 20 different areas are possible on a Smith chart. Only one TL can be used for both complex termination impedances, but the restrictions are inevitable. To solve them based on the allowed and forbidden regions, three complex impedances transformers are proposed additionally, connecting one TL, one open stub or one short stub to the original TL. For the verification, three complex impedance transformers, the termination impedances of which are located in forbidden regions, are fabricated and measured at a design frequency of 1 GHz. The measured $|S_{11}|$ of one transforming (68 + j42.5) into (85 + j17) Ω is −45.9 dB at 1 GHz, and the bandwidth with the 15-dB return loss is more than 100 %. One complex impedance transformer with (100-j30) and 50 Ω is designed to have 280 % bandwidth, as well.

INDEX TERMS Allowed and forbidden regions, frequency-dependent complex impedance transformers, complex impedance transformers with only one transmission-line section, complex termination impedances, bandwidth enhancement method for the complex impedance transformers.

I. INTRODUCTION

With the development of wireless communication systems, the impedance transformers to convert a certain impedance into another one are important for maximum power transfer. These transformers are exploited for impedance-transforming power dividers and combiners [1]–[6], wireless power transfer, energy harvest [7], antenna feeding lines, and power amplifiers. The simplest design is generally the most preferable for the engineering solution, and quarter-wave impedance transformers are suitable for this purpose. However, since input or output impedances of power transistors, transmitter- and receiver-coils for wireless power transfer systems and diodes for rectifiers are not always of real values, complex impedance transformers (CITs) to convert a complex impedance into another one are required.

Diverse CITs have been suggested and can be classified into six cases; the first case consisting of only one transmission-line section (TL) [8]–[11], the second one with one TL and stubs [12]–[14], the third one comprising of two TLs and stubs [15]–[20], the fourth one being composed of three TLs and stubs [21], [22], the fifth one made of only several TLs [23], and the last one with coupled TLs [24]–[26].

However, most of previous design methods [8], [12]–[17], [19]–[21], [23] cannot be possible for both complex termination impedances. All the conventional methods [8]–[26] cannot treat all possible complex termination impedances due to no systematic design method available, and the conventional designs [12]–[26] are more complicated than required. Among those methods, impedance transformers [8], [19] with each only a single TL are recommendable, due to powerful, simple, diverse applications and possible implementation of all the other conventional designs. However, those in [8] and [19] are possible only for one real termination impedance, or, not for both complex termination impedances.

To overcome the conventional problems [8], [19], the CITs with each only one TL are suggested in this paper for both complex termination impedances, and allowed and forbidden regions are suggested based on three mapping functions

The associate editor coordinating the review of this manuscript and approving it for publication was Mohamed Kheir.

which are for the first time derived in this paper. The allowed and forbidden regions are historically for the first time derived in [8], and followed by [19] and [27]. However, they [8] are possible only for one real and one complex termination impedances, those in [19] do not seem to be correct, referring to [20], and those in [27] is very briefly introduced with no completion. The design method for the both regions in this paper is quite different from the graphical method in [8] which cannot be possible for both complex termination impedances.

Even though the CITs with each only one TL are possible for both complex termination impedances, imaginary values of the characteristic impedances; too high value of characteristic impedances to fabricate; too long electrical length; or small bandwidths are inevitable. To solve those problems, three CITs are additionally proposed, adding one TL to the original TL, adding one open stub to the original TL, or adding one short stub to the original TL.

Since the Smith charts with both allowed and forbidden regions give all the information about the bandwidths [5], characteristic impedances and electrical lengths [3], [8] of the TL at a glance, they are very important for the effective designs without any additional complicated calculation or derivation process.

For the verification of suggested theory, three cases located in forbidden regions are measured. One of them is transforming $(68 + j42.5)$ into $(85 + j17)$ Ω. The measured return loss is 45.9 dB at a design frequency of 1 GHz, and the bandwidth with the 15-dB return loss is more than 100 %.

II. COMPLEX IMPEDANCE TRANSFORMER WITH ONLY ONE TRANSMISSION-LINE SECTION

A. IMPEDANCE DOMAIN ANALYSES

A CIT terminated in both complex impedances is depicted in Fig. 1(a). The CIT consists of only a single TL with the characteristic impedance of Z_C and the electrical length of Θ, and the two termination impedances of Z_L and Z_S are $Z_L = R_L + jX_L$ and $Z_S = R_S + jX_S$ where R_L and R_S are of positive real values, and X_L and X_S are of real values including 0.

If the two termination impedances are normalized to the real impedance R_S of Z_S in Fig. 1(b), they become to be $z_l = Z_L/R_S$ and $z_s = Z_S/R_S$, and the characteristic impedance of the TL is also to be $z_c = Z_C/R_S$. Reflection coefficients Γ_l, Γ_s and input impedance of z_{in_s} are indicated in Fig. 1(b). To have perfect matching at both complex termination impedances, the normalized termination impedances z_l and z_s should be located on a constant reflection coefficient circle drawn on a Smith chart, from which the following relation [8] holds;

$$|\Gamma_l| = |\Gamma_s|, \tag{1}$$

$$\Gamma_l = \frac{z_l - z_c}{z_l + z_c}, \quad \Gamma_s = \frac{z_s^* - z_c}{z_s^* + z_c} \tag{1a}$$

where $z_l = r_l + jx_l$ and $z_s = 1 + jx_s$. From the relations in (1), the normalized characteristic impedance of z_c is derived as

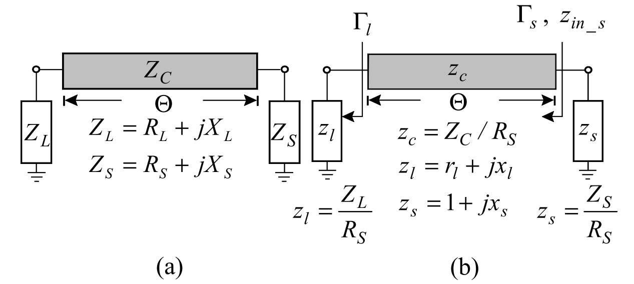

FIGURE 1. CITs. (a) Without normalization. (b) Termination and characteristic impedances normalized to R_S.

$$z_c = \sqrt{\frac{r_l |z_s|^2 - |z_l|^2}{1 - r_l}} \tag{2}$$

The design formula in (2) may also be obtained by substituting z_l and z_s into [8, eq. (2)] or [9, 31-9]. The input impedance z_{in_s} in Fig. 1(b) is

$$z_{in\_s} = z_c \frac{z_l + jz_c tan\Theta}{z_c + jz_l tan\Theta} \tag{3}$$

For the perfect matching at z_s in Fig. 1(b), $z_{in\_s} = z_s^*$ should be, from which the electrical length of Θ may be found as

$$tan\Theta = z_c \frac{r_l - 1}{r_l x_s - x_l} \tag{4}$$

For the solution to z_c in (2), z_c^2 should be of positive real values, which leads to

$$0 < r_l < 1; \left(r_l - \frac{|z_s|^2}{2}\right)^2 + {x_l}^2 < \frac{|z_s|^4}{4} \tag{5a}$$

$$r_l > 1; \left(r_l - \frac{|z_s|^2}{2}\right)^2 + {x_l}^2 > \frac{|z_s|^4}{4} \tag{5b}$$

$$r_l = 1; \text{no solution} \tag{5c}$$

where two cases of $0 < r_l < 1$ and $r_l > 1$ are available, and no solution to z_c exists, when $r_l = 1$ in (5c). Depending on the values of $|z_s|^2$, the two cases with $|z_s|^2 > 1$ and $|z_s|^2 = 1$ are plotted in Fig. 2(a) and (b), respectively where hatched regions are allowed regions that allow positive real characteristic impedances of z_c in (2) with only one TL.

B. REFLECTION COEFFICIENT DOMAIN ANALYSES

For the analyses on a Smith chart, three boundary functions defined in the impedance domain need to be mapped onto a Smith chart. The three are found from the equations in (2), (4), (5), which are

$$f_1(r_l, x_l): \left(r_l - \frac{|z_s|^2}{2}\right)^2 + {x_l}^2 - \frac{|z_s|^4}{4} = 0 \tag{6a}$$

$$f_2(r_l, x_l): r_l - 1 = 0 \tag{6b}$$

$$f_3(r_l, x_l): r_l - \frac{x_l}{x_s} = 0 \tag{6c}$$

The two in (6a) and (6b) are for the characteristic impedance of z_c in (2), and the two in (6b) and (6c) with $x_s \neq 0$ are for the electrical length of Θ from (4). By the conformal mapping of $\Gamma_l = (z_l - 1)\,/\,(z_l + 1)$, real and imaginary parts of the reflection coefficient $\Gamma_{rl} + j\Gamma_{il}$ [8, eq.(7)] are written as

$$\Gamma_{rl} = \frac{(r_l^2 - 1) + x_l^2}{(1 + r_l)^2 + x_l^2} \tag{7a}$$

$$\Gamma_{il} = \frac{2x_l}{(1 + r_l)^2 + x_l^2}, \tag{7b}$$

where $z_l = r_l + jx_l$, also,

$$\left(\Gamma_{rl} - \frac{r_l}{1 + r_l}\right)^2 + \Gamma_{il}^2 = \left(\frac{1}{1 + r_l}\right)^2 \tag{7c}$$

$$(\Gamma_{rl} - 1)^2 + \left(\Gamma_{il} - \frac{1}{x_l}\right)^2 = \left(\frac{1}{x_l}\right)^2 \tag{7d}$$

The equations in (7) indicate that a circle in z_l- domain is converted into another circle in Γ_l- domain on a Smith chart, a line is also transformed into a circle, and the conformal mapping of z_l into Γ_l is 1:1 mapping. Letting the mapping function of $f_1\,(r_l, x_l)$ be $G_{f_1}\,(\Gamma_{rl}, \Gamma_{il})$, it is necessary to know two points together with a radius converted from $f_1\,(r_l, x_l)$ defined in z_l- domain in (6a), because they are sufficient to define a circle. The two are $A\,(0, 0)$ and $B\,(0, 2C)$ in Fig. 2(a) where C is the center of the circle. Substituting $(r_l, x_l)_A = (0, 0)$ into the two in (7a) and (7b) gives

$$(r_l, x_l)_A = (0, 0) \rightarrow (\Gamma_{rl}, \Gamma_{il})_A = (-1, 0) \tag{8}$$

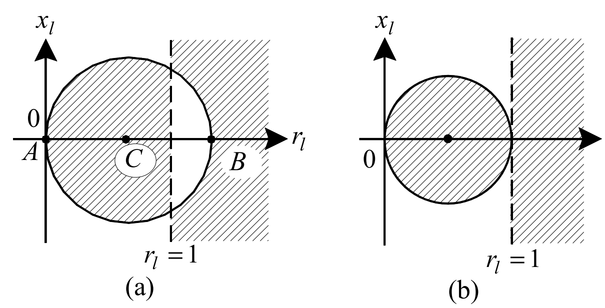

FIGURE 2. **Hatched allowed regions. (a) $|z_s|^2 > 1$. (b) $|z_s|^2 = 1$.**

The value of $2C$ at $B(2C,\ 0)$ in Fig. 2(a) is $|z_s|^2$ from (6a), which is converted into

$$(r_l, x_l)_B = \left(|z_s|^2, 0\right) \rightarrow (\Gamma_{rl}, \Gamma_{il})_B = \left(\frac{|z_s|^2 - 1}{|z_s|^2 + 1}, 0\right) \tag{9}$$

The radius RG_{f_1} of the circle of $G_{f_1}\,(\Gamma_{rl}, \Gamma_{il})$ is obtained from

$$RG_{f_1} = \frac{\Gamma_{rl\_B} - \Gamma_{rl\_A}}{2} \tag{10}$$

where Γ_{rl_A} and Γ_{rl_B} are real parts of $(\Gamma_{rl}, \Gamma_{il})_A$ and $(\Gamma_{rl}, \Gamma_{il})_B$ in (8) and (9), respectively.

The function of $G_{f_1}\,(\Gamma_{rl}, \Gamma_{il})$ is therefore obtained as

$$f_1\,(r_l, x_l) \rightarrow G_{f_1}\,(\Gamma_{rl}, \Gamma_{il})$$

$$G_{f_1} : \left(\Gamma_{rl} + \frac{1}{1 + |z_s|^2}\right)^2 + \Gamma_{il}^2 - \left(\frac{|z_s|^2}{1 + |z_s|^2}\right)^2 = 0 \tag{11}$$

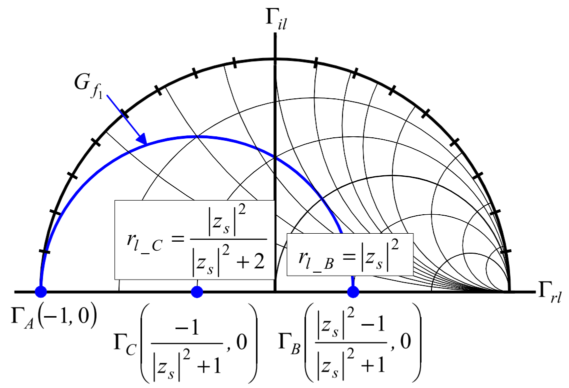

FIGURE 3. **Precise description of a half circle of $G_{f_1}\,(\Gamma_{rl}, \Gamma_{il})$.**

A half circle of $G_{f_1}\,(\Gamma_{rl}, \Gamma_{il})$ is represented in Fig. 3 where the circle passes through Γ_A and Γ_B, and the center of the circle is Γ_C. The real values of Γ_C and Γ_B are $-1/(1 + |z_s|^2)$ and $(|z_s|^2 - 1)/(1 + |z_s|^2)$ as expressed. Substituting those real values of Γ_C and Γ_B into (7a) with $x_l = 0$, r_{l_C} and r_{l_B} are derived inversely as

$$r_{l\_C} = \frac{|z_s|^2}{|z_s|^2 + 2}, \quad r_{l\_B} = |z_s|^2 \tag{12}$$

where r_{l_C} and r_{l_B} are the corresponding real resistance values at Γ_C and Γ_B, respectively, in Fig. 3. In other words, for example, if $z_s = 1 + j$ is given, the function of $G_{f_1}\,(\Gamma_{rl}, \Gamma_{il})$ is a circle passing through two points $(r_{l\_A} = 0)$ and $(r_{l\_B} = 2)$ on $\Gamma_{rl}-$ axis in (8) and (9), and the center of the circle is $r_{l\_C} = 1/2$ as in (12). When $z_s = 1 + j$, the center of the circle in the impedance domain in Fig. 2(a) is $(r_l, x_l)_C = (1, 0)$, but the center of G_{f_1} in the reflection domain is not $(r_l, x_l)_C = (1, 0)$ but $(r_l, x_l)_C = (1/2, 0)$. That is, 1:1 mapping can be achieved only between the two circles in the impedance and reflect domains.

The mapping function of $f_2\,(r_l, x_l)$ in (6b) is easily obtained by substituting $r_l = 1$ into (7c) to give

$$f_2\,(r_l, x_l) \rightarrow G_{f_2}\,(\Gamma_{rl}, \Gamma_{il})$$

$$G_{f_2} : \left(\Gamma_{rl} - \frac{1}{2}\right)^2 + \Gamma_{il}^2 - \left(\frac{1}{2}\right)^2 = 0 \tag{13}$$

The two functions in (11) and (13) are valid for both complex termination impedances.

With $|x_s|$ varying, the circles expressing two functions of $G_{f_1}\,(\Gamma_{rl}, \Gamma_{il})$ and $G_{f_2}\,(\Gamma_{rl}, \Gamma_{il})$ are plotted in an impedance Smith chart in Fig. 4. The circle of $G_{f_2}(\Gamma_{rl}, \Gamma_{il})$ is a fixed $r_l = 1$ circle. The circles of $G_{f_1}(\Gamma_{rl}, \Gamma_{il})$ are dependent on

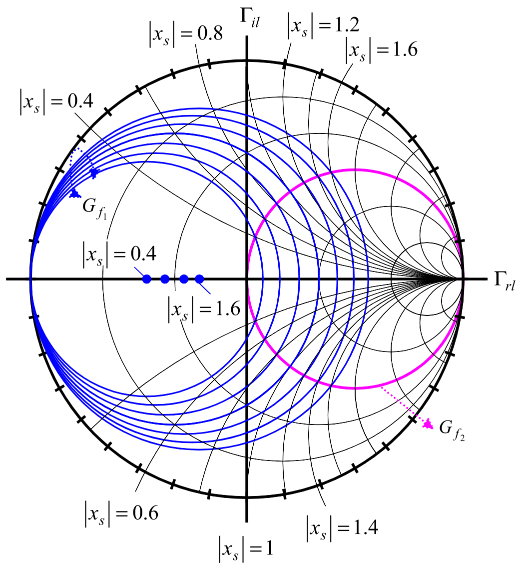

FIGURE 4. Family of G_{f_1} $(\Gamma_{rl}, \Gamma_{il})$ and G_{f_2} $(\Gamma_{rl}, \Gamma_{il})$ circles.

x_s and meet $G_{f_2}(\Gamma_{rl}, \Gamma_{il})$ at two points, $1 \pm jx_s$. If the value of $|x_s|$ is larger, the radius of the $G_{f_1}(\Gamma_{rl}, \Gamma_{il})$ is greater, which may be known from Fig. 3. Independently of the values of $|x_s|$, the family of G_{f_1} are passing through three points of $(\Gamma_{rl}, \Gamma_{il}) = (-1, 0)$ and $1 \pm jx_s$. With $|x_s|$ larger, the centers of the circles of G_{f_1} are closer to the origin of the Smith chart. The two functions in (11) and (13) are independent of the sign of x_s, but the electrical lengths of Θ are dependent on the sign of x_s. In a similar way, the mapping function of f_3 (r_l, x_l), G_{f_3} $(\Gamma_{rl}, \Gamma_{il})$ is found as

$$f_3\,(r_l, x_l) \rightarrow G_{f_3}\,(\Gamma_{rl}, \Gamma_{il})$$

$$G_{f_3} : \Gamma_{rl}^2 + \left(\Gamma_{il} + \frac{1}{x_s}\right)^2 - \left(1 + \frac{1}{x_s^2}\right) = 0 \quad (14)$$

By varying x_s, the family of circles of G_{f_3} $(\Gamma_{rl}, \Gamma_{il})$ are drawn in Fig. 5 where the cases with $x_s > 0$ are in Fig. 5(a), while those with $x_s < 0$ in Fig. 5(b). The family of circles meets z_s, and as the value of $|x_s|$ approaches to infinite, the center of circles G_{f_3} $(\Gamma_{rl}, \Gamma_{il})$ goes to the origin of the impedance Smith chart, and the radius becomes to be unity. Since the behavior of three circles in (11), (13) and (14) is dependent on $|z_s|^2$, the cases of $|z_s|^2 > 1$ and $|z_s|^2 = 1$ will be discussed further.

C. ALLOWED AND FORBIDDEN REGIONS

As far as x_s is of real values, $|z_s|^2 \geq 1$ is always satisfied, and three cases, $x_s > 0$, $x_s < 0$ ($|z_s|^2 > 1$) and $x_s = 0$ ($|z_s|^2 = 1$) are possible. The three cases are different from each other, which should be studied differently. The conditions for a real value of z_c are

$$G_{f_1}\,(\Gamma_{rl}, \Gamma_{il}) < 0 \quad \textit{and} \quad G_{f_2}\,(\Gamma_{rl}, \Gamma_{il}) > 0 \quad (15a)$$

$$G_{f_1}\,(\Gamma_{rl}, \Gamma_{il}) > 0 \quad \textit{and} \quad G_{f_2}\,(\Gamma_{rl}, \Gamma_{il}) < 0 \quad (15b)$$

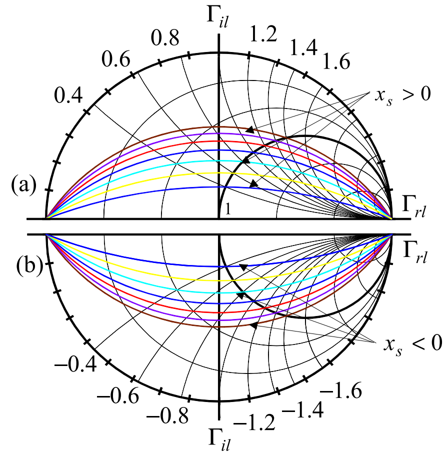

FIGURE 5. Family of G_{f_3} $(\Gamma_{rl}, \Gamma_{il})$ circles. (a) $x_s > 0$. (b) $x_s < 0$.

The condition in (15a) for the reflection domain on the Smith chart corresponds to that in (5a) in the impedance domain, while that in (15b) corresponds to that in (5b). The regions satisfying (15) with $x_s > 0$ are illustrated in Fig. 6(a). The two circles of G_{f_1} $(\Gamma_{rl}, \Gamma_{il})$ and G_{f_2} $(\Gamma_{rl}, \Gamma_{il})$ meet at two points, one of which is z_s and another of which is z_s^*. The third circle of G_{f_3} $(\Gamma_{rl}, \Gamma_{il})$ passes through z_s and determines the sign of the electrical lengths of Θ. If a complex impedance of z_l is located within the hatched region, real value of z_c is possible, and therefore a single TL in Fig. 1(b) can transform z_l into z_s. Due to the fundamental reason, the hatched region in Fig. 6(a) is called allowed region which may be divided into four I^+, II^+, III^+ and IV^+ where the letter of "A" of AI^+, AII^+, AIII^+ and AIV^+ indicates allowed regions, the sign of $+$ in the superscript means that x_s is positive, and $+$ or – sign located next to those is the sign of electrical length of Θ. The positive or negative electrical length of Θ means $\Theta < 90°$ or $\Theta > 90°$, respectively. If z_l is located on the circle of G_{f_3} $(\Gamma_{rl}, \Gamma_{il})$, $\Theta = 90°$.

With a given $x_s < 0$, the conditions for a real value of z_c are the same as those in (15), but the function of G_{f_3} is different from that with $x_s > 0$. Therefore each region is also different. The allowed regions with $x_s < 0$ is illustrated in Fig. 6(b) where the three circles meet at z_s. The sign of – in the superscript means that x_s is negative. Compared to the case with $x_s > 0$, the regions of AI^- and AII^- are bigger than those of AI^+ and AII^+. The sign of $+$ or – located next to those is also the sign of electrical length of Θ. The case with $x_s = 0$ is described in [8, Fig. 6(c)]. The outside of the allowed regions is forbidden regions, and two types are available. They are in Fig. 6(d) and (e) where the sign of $+$ or – in the superscript indicates the sign of x_s, as well.

III. SOLUTION TO RESTRICTIONS

In general, the two equations (2) and (4) may be used for the CITs terminated in both complex impedances. However, there are restrictions, and four of them are imaginary values of z_c, too high value of the characteristic impedance of

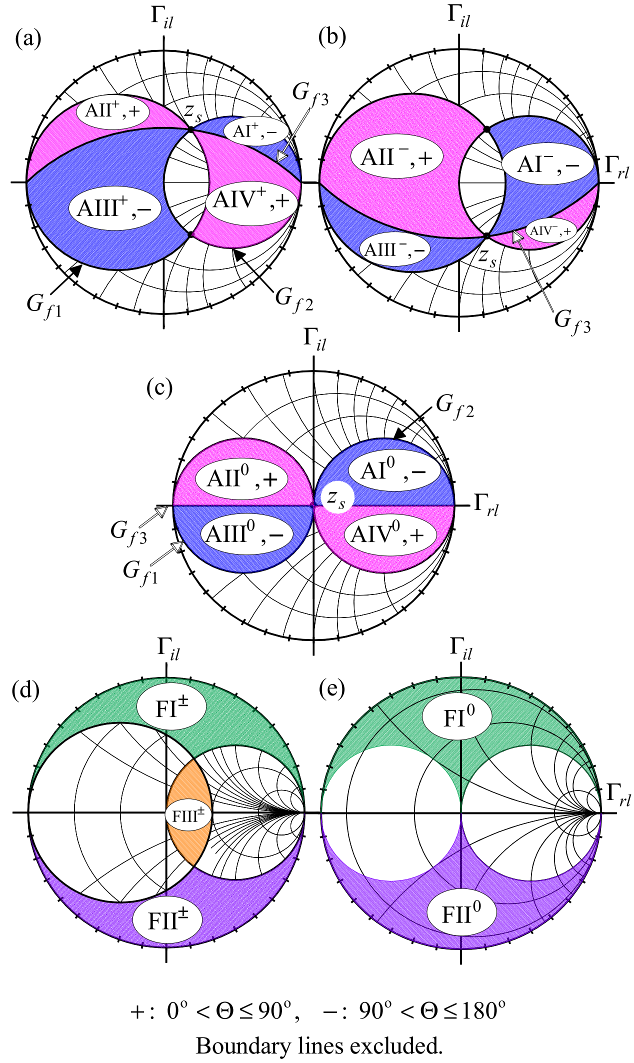

FIGURE 6. Allowed and forbidden regions. (a) Allowed regions with $x_s > 0$. (b) Allowed regions with $x_s < 0$. (c) Allowed regions with $x_s = 0$. (d) Forbidden regions with $x_s \neq 0$. (e) Forbidden regions with $x_s = 0$.

z_c to fabricate, too long electrical length of Θ and small bandwidths. To solve those problems, allowed and forbidden regions are required. For example, if the load of z_l is located in a forbidden region, the resulting z_c is of imaginary value. In this case, the load of z_l should be moved into one of allowed regions where the electrical length of the CIT in Fig. 1(b) is less than 90° for the compact designs.

For this purpose, any circuit to transform the original complex impedance of z_l into a wanted region is necessary, and the simplest circuits are those made by only one TL. They are a TL, an open stub and a short stub in Fig. 7 where the TL has the characteristic impedance of z_t and the electrical length of Θ_t in Fig. 7(a), while an open stub with the characteristic impedance of z_o and the electrical length of $\Theta_\circ$ and a short stub with z_{sh} and Θ_{sh} are indicated in Fig. 7(b) and (c), respectively.

In this case, the complex load of z_l is transformed into three input impedances of z_{in_t}, z_{in_o} and z_{in_sh} as shown in Fig. 7,

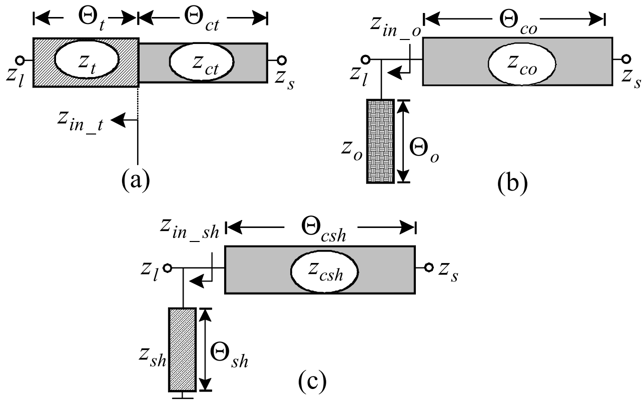

FIGURE 7. Three asymmetric CITs with two elements. (a) A TL added (CVT). (b) An open stub added (CCTU). (c) A short stub added (CCTD).

which are

$$z_{in\_t} = \frac{z_t^2 r_l sec^2\Theta_t}{(z_t - x_l\tan\Theta_t)^2 + r_l^2\tan^2\Theta_t} + jz_t\frac{z_t^2 tan\Theta_t + z_t x_l\left(1 - tan^2\Theta_t\right) - |z_l|^2\tan\Theta_t}{(z_t - x_l\tan\Theta_t)^2 + r_l^2\tan^2\Theta_t} \tag{16a}$$

$$z_{in\_o} = z_o\frac{z_o r_l + j\left(z_o x_l - |z_l|^2\tan\Theta_\circ\right)}{(z_o - x_l\tan\Theta_\circ)^2 + r_l^2\tan^2\Theta_\circ} \tag{16b}$$

$$z_{in\_sh} = z_{sh}\frac{z_{sh} r_l + j\left(z_{sh} x_l + |z_l|^2\cot\Theta_s\right)}{(z_{sh} + x_l\cot\Theta_s)^2 + r_l^2\cot^2\Theta_s} \tag{16c}$$

Then, the characteristic impedances of z_{ct}, z_{co} and z_{csh} and the electrical lengths of Θ_{ct}, Θ_{co} and Θ_{csh} of the TLs in Fig. 7 are calculated using the two equations in (2) and (4) to give

$$z_{ci} = \sqrt{\frac{a_i|z_s|^2 - |z_{in\_i}|^2}{1 - a_i}} \tag{17a}$$

$$tan\Theta_{ci} = z_{ci}\frac{a_i - 1}{a_i x_s - b_i} \tag{17b}$$

where i is meant as t, o and sh, and a_i and b_i are real and imaginary values of z_{in_i} in (16).

To determine the TL, the open or short stubs in Fig. 7 for the solutions, the defined allowed and forbidden regions are needed, which will be discussed further. Since the asymmetric impedance transformers [3] are named based on how to move the loads, the CITs in Fig. 7(a), (b) and (c) can be named CVT, CCTU and CCTD, respectively where CCTU or CCTD means that the admittance load is moved upwards or downwards along a constant conductance circle on the Smith chart.

A. IMAGINARY VALUES OF CHARACTERISTIC IMPEDANCES

For an example of $z_l = (0.8 + j0.5)\ \Omega$ with a given $z_s = (1 + j0.2)\ \Omega$, substituting the two into eq. (2) gives an imaginary value, which indicates the transformation of z_l into z_s with only one TL is impossible. To make it feasible, one of the three circuits in Fig. 7 may be used.

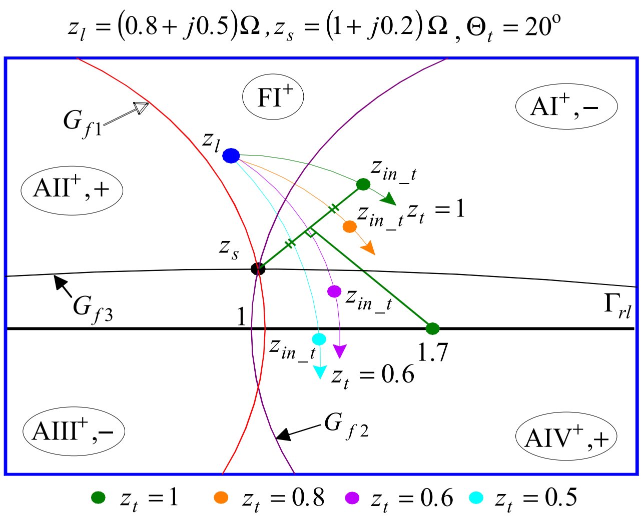

FIGURE 8. Illustration of an example with a forbidden region of FI$^+$.

To solve this problem, the three functions in (11), (13) and (14) are plotted in Fig. 8 where the complex load of z_s is located at the point where the three functions meet, and the load of z_l is located in the forbidden region of FI$^+$. To make it feasible, the load of z_l should be moved into one of allowed regions where the resulting electrical length of Θ_{ct}, Θ_{co} or Θ_{csh} in Fig. 7 is less than 90°. The possible allowed region is AII$^+$, $+$ or AIV$^+$, $+$ in Fig. 6(a). For this, the CVTs in Fig. 7(a) and the CCTDs in Fig. 7(c) are good candidates, and the CVTs will be discussed.

Even if the input impedance of z_{in_t} in Fig. 7(a) is changed with the TL with z_t and Θ_t, the three functions are the same as far as z_s is fixed. Therefore, the Smith chart in Fig. 8 is for $z_{in\_t} = a_t + jb_t$ where a_t and b_t are real and imaginary values of z_{in_t} in (16a) and Fig. 7(a).

With fixing Θ_t at 20° and with varying z_t in Fig. 7(a), the resulting input impedances of z_{in_t} are described in Fig. 8. When $z_t = 1$, the input impedance of z_{in_t} is still in the region of AI$^+$, $-$ and therefore the electrical length of Θ_{ct} in Fig. 7(a) is negative, or, greater than 90°. When $z_t = 0.6$, the input impedance of z_{in_t} is in the region of AIV$^+$, $+$ and therefore the electrical length of Θ_{ct} is positive, but close to 90°, because the point of z_{in_t} with $z_t = 0.6$ is located close to the function of G_{f3}. When $z_t = 0.5$, the input impedance of z_{in_t} is located farther from the function of G_{f3}. Therefore, the electrical length of Θ_{ct} should be less than that with $z_t = 0.6$. In this way, the three functions give

TABLE 1. Design Parameters of CVTs in Fig. 7(a) for FI$^+$.

$z_l =$ (0.8+j0.5) Ω, $z_s =$ (1+j0.2) Ω, $\Theta_t = 20^\circ$			
z_t(Ω)	z_{in_t} (Ω)	z_{ct}(Ω)	Θ_{ct}(°)
0.5	1.218 - j0.0432	1.0018	37.31
0.6	1.257 + j0.1557	1.0749	70.88
0.8	1.242 + j0.4388	1.3535	120.13
1	1.2017 + j0.6284	1.7093	138.34

all the information for z_{ct} and Θ_{ct}, and the detailed design parameters are given in Table 1. Without calculations, the characteristic impedances of z_{ct} can be known approximately. For the case of $z_t = 1$ in Fig. 8, the perpendicular bisector of the line connecting z_s and its corresponding z_{in_t} meets the real axis of Γ_{rl} at one point. The point indicates the characteristic impedance of z_{ct}, referring to [3, Fig. 5], [8, Figs. 3,4] and $z_{ct} = 1.709$ in Table 1. In this way, even when the resulting value from (2) is imaginary, the CITs are possible by adding only one element more.

B. MEASUREMENTS OF THE CASES IN FORBIDDEN REGIONS

Several CVTs in Fig. 7(a), the termination impedances of z_l of which are located in forbidden regions, are fabricated on a substrate (RT/Duroid 5880,$\varepsilon_r = 2.2$, $H = 20$ mil). In this case, the load located in the forbidden region FI$^+$ is $z_l =$ (0.8 + j0.5) Ω with $z_s =$ (1 + j0.2) Ω as exemplified in Fig. 8, that in the forbidden region FII$^-$ is $z_l =$ (0.9-j0.6) Ω with $z_s =$ (1-j0.3) Ω, and that in the forbidden region of FIII$^+$ is $z_l =$ (1.4 + j0.7) Ω with $z_s =$(1 + j1) Ω. The forbidden regions mean that the characteristic impedances of z_c are of imaginary values when substituting those (z_l and z_s) into (2). The design parameters are collected in Table 2 where R_S is chosen depending on available resistance value, and Z_L, Z_S, Z_T and Z_{Ct} are $z_l * R_S$, $z_s * R_S$, $z_t * R_S$ and $z_{ct} * R_S$, respectively.

TABLE 2. Design Parameters of CVTs in Fig. 7(a) for Forbidden Regions.

z_l	z_s	z_t, Θ_t	z_{ct}, Θ_{ct}	R_S
0.8+j0.5	1+j0.2	0.6, 35°	1.3, 17.56°	85.0
0.9-j0.6	1-j0.3	2.5, 20°	1.1, 20.11°	47.78
1.4+j0.7	1+j	1.85, 15°	0.77, 35.34°	65

Z_L	Z_S	Z_T, Θ_t	Z_{Ct}, Θ_{ct}
68+ j42.5	85+j17	51, 35°	110.06, 17.56°
43-j28.67	47.78-j14.33	119.4, 20°	50.94, 20.11°
91+ j45.5	65+j65	120.25, 15°	50.19, 35.34°

The fabricated impedance transformers are demonstrated in Fig. 9 (a), (b) and (c) where the case of forbidden region of FI$^+$ is in Fig. 9(a), while those with forbidden regions II$^-$ and III$^+$ are in Fig. 9(b) and (c), respectively. The real values of Z_L are fabricated with available chip resistors of R_L, and the imaginary values of Z_L are realized with available chip inductor or capacitor together with TLs. The complex impedance of $Z_L =$ (68 + j42.5) Ω in Fig. 9(a) is realized with a chip resistor with 68 Ω, a TL with the characteristic impedance of 50 Ω and the electrical length of 8.39° at 1 GHz, and a chip inductor of 4.7 nH. That of $Z_L =$ (43-j28.67) Ω in Fig. 9(b) is composed of a chip resistor with 43 Ω, a TL with 60 Ω and 6.13° and a chip capacitor with 4.3 pF. That of $Z_L =$ (91 + j45.5) Ω in Fig. 9(c) is made of a chip resistor with 91 Ω, a TL with 70 Ω and 8.43°, and a chip inductor with 5.1 nH. Each TL is used for trimming required capacitance or inductance values. The TLs with

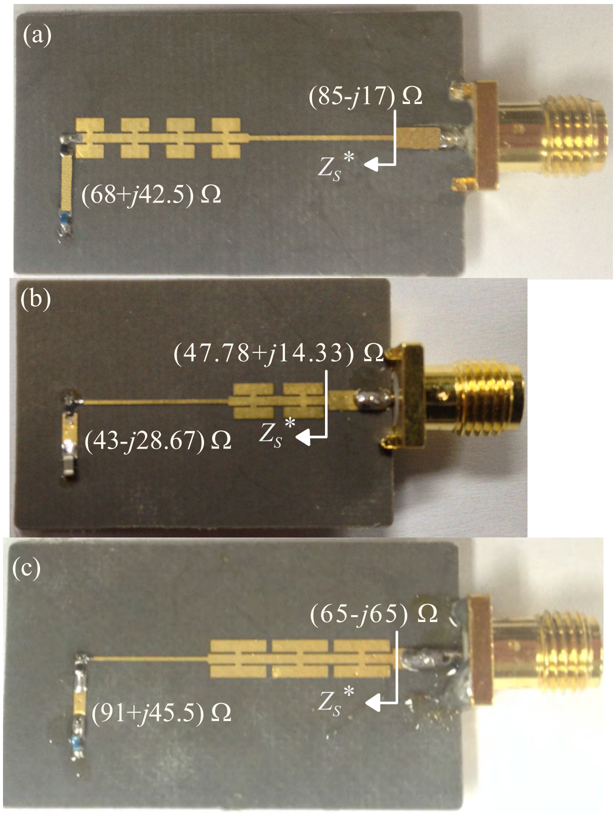

FIGURE 9. Fabricated CVTs for Forbidden regions. (a) FI$^+$. (b) FII$^-$. (c) FIII$^+$.

low characteristic impedances in Table 2 are further reduced by use of MT (modified T-types) [28], [29, Fig. 6(b) with $\Theta_a = 0$]. The TL with $Z_T = 51\ \Omega$ and $\Theta_t = 35°$ in Table 2 is reduced to 22.34° long with $N = 4$ in [28] and [29] as shown in Fig. 9(a). That with $Z_{Ct} = 50.94\ \Omega$ and $\Theta_{ct} = 20.11°$ is reduced to 12.82° long with $N = 2$ as illustrated in Fig. 9(b). That with $Z_{Ct} = 50.19\ \Omega$ and $\Theta_{ct} = 35.34°$ is reduced to 22.22° long with $N = 3$ as demonstrated in Fig. 9(c).

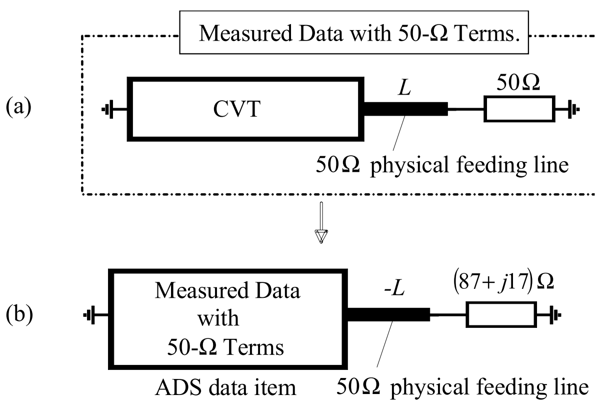

FIGURE 10. Measured data transformation. (a) 50-Ω termination impedances. (b) Non 50-Ω termination impedance.

The input impedances indicated by the arrows in Fig. 9 are complex conjugates of Z_S for perfect matching. The termination impedances of Z_S in Fig. 9 are not 50 Ω, and therefore the 50-measurement system may not be suitable. One of ways for the measurements is as follows. Letting the targeting circuit for the measurements be a circuit (CVT) in Fig. 10(a), the characteristics of the CVT are not changed by the termination impedances. That is, impedance, admittance and *ABCD* parameters of the CVT are not changed by the termination impedances [4], but only the scattering parameters are changed by the termination impedances. The CVT is measured in the form in Fig. 10(a) where the characteristic impedance and the physical length of the feeding line are assumed to be 50 Ω and L, respectively. After measuring the scattering parameter of the CVT with the 50-Ω termination impedances, the measured data are saved in the ADS data item in Fig. 10(b). Since the saved data contain the feeding lines, the feeding line effect should be removed by adding a TL with the characteristic impedance of 50 Ω but the physical length of -L. For the measured data in Fig. 10(b), after terminating the CVT in the real termination impedance of Z_S, or, $(87 + j17)\ \Omega$, if it is simulated once more, the converted data are obtained and can be the measured data with Z_S-termination impedance.

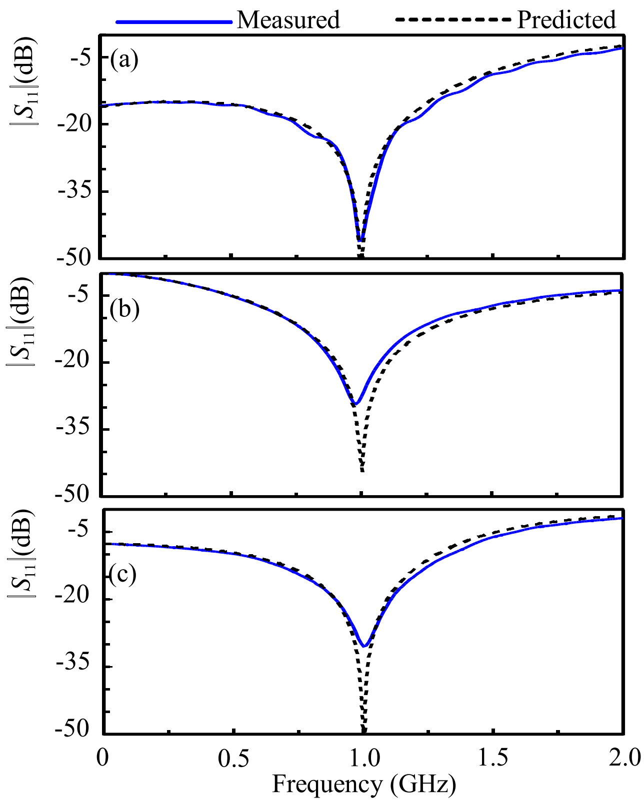

FIGURE 11. Measured frequency responses of CVTs. (a) FI$^+$. (b) FII$^-$. (c) FIII$^+$.

The frequency responses measured and predicted are compared in Fig. 11 where the cases with forbidden regions FI$^+$, FII$^-$ and FIII$^+$ are in Fig. 11(a), (b) and (c), respectively. The measured scattering paramters of $|S_{11}|$ at 1 GHz are −45.9, −27.65 and −29.7 dB, respectively. The bandwidth with 15-dB return loss of the CVT in forbidden region I in Fig. 11(a) is more than 100 %, and quite good agreements between measured and predicted results are achieved.

Even though the imaginary parts of the termination impedances of Z_S and Z_L are frequency-dependent, since all the solutions to the characteristic impedances and electrical lengths are valid only at a design frequency, the frequency responses with the fixed Z_S and Z_L at f_o, a design frequency, are correct to verify the suggested theory, referring to [6, Fig. 25].

C. TOO HIGH CHARACTERISTIC IMPEDANCES AND TOO LONG ELECTRICAL LENGTHS

Another example is that characteristic impedance or electrical length is too high or too long to fabricate. For the example of a complex load of $z_l = (1.32 + j2.89)\ \Omega$ with a given $z_s = (1 + j)\ \Omega$, the load of z_l is located in $\mathrm{AI}^+, -$. Substituting the two of z_l and z_s into eqs. (2) and (4) gives $\Theta = -44.53°$, or, 134.47° and $z_c = 4.83\ \Omega$. If the normalized impedance of R_S is 50 Ω, the real characteristic impedance becomes 4.83∗50 Ω which is very difficult to fabricate with a general microstrip technology. Furthermore, the electrical length is too long $(180 + \Theta)$, 134.77°.

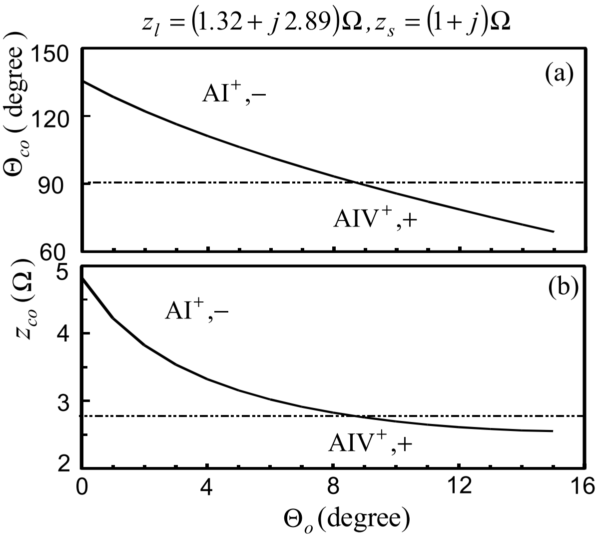

FIGURE 12. Variations of electrical lengths of $\Theta_{c\circ}$ and characteristic impedance of z_{co} using the CCTU in Fig. 7(b) for $z_l = (1.32 + j2.89)\ \Omega$ and $z_s = (1 + j)\ \Omega$. (a) $\Theta_{c\circ}$. (b) z_{co}.

To make the unfeasible characteristic impedance viable and to reduce the size, to move the load of z_l into $\mathrm{AIV}^+, +$ is needed. For this, the CCTU in Fig. 7(b) is an alternative choice. Fixing $z_o = 1$ and varying Θ_o, the calculation results of Θ_{co} and z_{co} in Fig. 7(b) are plotted in Fig. 12 where the electrical lengths of Θ_{co} are in Fig. 12(a), while the characteristic impedances of z_{co} in Fig. 12(b).

With the open stub longer, Θ_{co} and z_{co} decrease in Fig. 12, and when the open stub is 8.84° long, the load of z_{in_o} in Fig. 7(b) is located on G_{f_3}, leading to $z_{co} = 2.76$ and $\Theta_{c\circ} = 90°$. When open stubs are 12° and 15° long, the values of z_{co} and $\Theta_{c\circ}$ can be calculated as $(z_{co}, \Theta_{c\circ}) = (2.61, 78.59°)$ and $(2.55, 68.76°)$, respectively. Even with the normalized impedance of 50 Ω, the characteristic impedance of $z_{co} = 2.76$ can be feasible with microstrip technology. Three cases with the open stub lengths of $\Theta_\circ = 8.84°$, 12° and 15° were simulated at the design frequency of 1 GHz, and the frequency responses are compared in Fig. 13 where the frequency responses for three cases are about the same, even when the sizes (electrical lengths) are different from each other. The simulation results in Figs. 12 and 13 demonstrate that adding just an open stub in Fig. 7(b) makes the unfeasible impedance transformer feasible along with the size reduction effect.

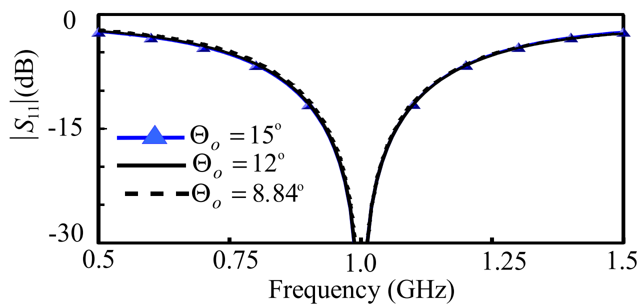

FIGURE 13. Frequency responses of CCTUs for $\Theta_\circ = 8.84°$, 12° and 15°.

D. SMALL BANDWIDTHS

When the bandwidth of the CIT with only one TL is considered to be small, the three CITs in Fig. 7 can be used as well. One case with $Z_L = (100\text{-}j30)\ \Omega$ at f_0 and $Z_S = 50\ \Omega$ in [8, Fig. 20(a)] can be exemplified. The complex impedance of Z_L is located in $\mathrm{AIV}^0, +$ in Fig. 6(c), leading to real value of Z_C and the electrical length of Θ less than 90°. Using the two design formulas in (2) and (4), the values of Z_C and Θ in Fig. 1 can be calculated as $Z_C = 76.8\ \Omega$ and $\Theta = 68.7°$. In this case, if the bandwidth is not thought to be desirable, the CVT in Fig. 7(a) can be used to increase the bandwidth.

Varying Z_T and fixing Θ_t at 38.86°, the design parameters for the CVTs in Fig. 7(a) are listed in Table 3 where $Z_T = z_t R_S$ and $Z_{Ct} = z_{ct} R_S$. The frequency responses of the CVTs in Table 3 are plotted in Fig. 14 where the complex termination impedance Z_L is frequency-dependent such as $Z_L = [100 - j30 \left\{\cot\left(\frac{\pi}{4}\frac{f}{f_0}\right)\right\}]\ \Omega$.

TABLE 3. Design Parameters of CVTs for $\Theta_t = 38.86°$.

$Z_T(\Omega)$, $Z_{Ct}(\Omega), \Theta_{ct}$	$Z_T(\Omega)$, $Z_{Ct}(\Omega), \Theta_{ct}$	$Z_T(\Omega)$, $Z_{Ct}(\Omega), \Theta_{ct}$
80 Ω, 71.1 Ω, 37.33°	82.1 Ω, 68.6 Ω, 41.6°	84 Ω, 66.9 Ω, 45.4°
86 Ω, 65.6 Ω, 49.4°	88 Ω, 64.6 Ω, 53.4°	90 Ω, 63.8 Ω, 57.2°

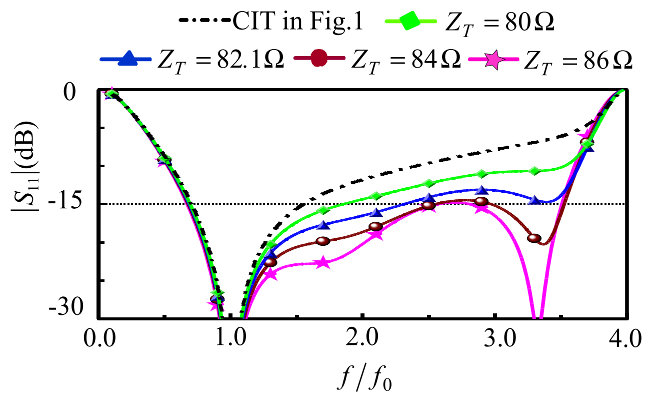

FIGURE 14. Frequency responses of CVTs in Fig. 7(a).

TABLE 4. Design Parameters for CVTs in Fig. 15(b) Fixing at $Z_T = 82.1\ \Omega$, $\Theta_t = 38.86°$ and $Z_o = 50\ \Omega$.

$Z_m(\Omega)$, Θ_m Θ_o	$Z_m(\Omega)$, Θ_m Θ_o	$Z_m(\Omega)$, Θ_m Θ_o
84 Ω, 17.24° 9.15°	82.1 Ω, 17.61° 8.3°	79 Ω, 18.26° 6.78°
76 Ω, 18.93° 5.11°	73 Ω, 19.65° 3.23°	70 Ω, 20.42° 1.09°

The frequency response of the CIT with only one TL in Fig. 1 is expressed with a dotted line, while those of the CVTs in Fig. 7(a) for $Z_T = 80$, 82.1, 84 and 86 Ω are solid lines with the symbols. Referring to the design parameters in Table 3, higher values of Z_T give longer electrical lengths (Θ_{ct}). The 15-dB return-loss bandwidth is the widest with $Z_T = 86$ Ω, and the bandwidth with $Z_T = 82.1\Omega$ is not so desirable.

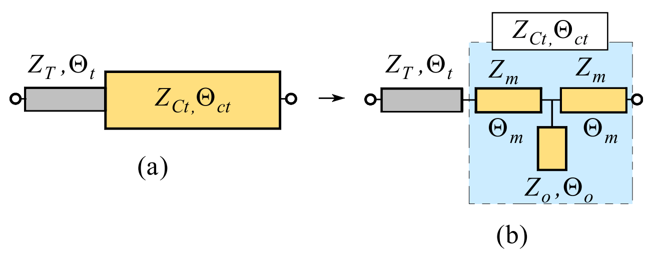

FIGURE 15. CVTs. (a) CVTs in Fig. 7(a). (b) Other type of CVT.

However, if converting the TL with Z_{Ct}, Θ_{ct} into a T-type with $N = 1$ [28], [29], the bandwidths can be enlarged. Fig. 15 shows converting the TL with Z_{Ct}, Θ_{ct} into a T-type where the T-type in Fig. 15(b) consists of two identical TLs with the characteristic impedance of Z_m and the electrical length of Θ_m and an open stub with Z_o and Θ_o. Varying Z_m and fixing Z_o at 50 Ω, the design parameters for $Z_T = 82.1$ Ω and $\Theta_t = 38.86°$ in Table 3 are listed in Table 4 where the design parameters for $Z_T = Z_m = 82.1\Omega$ are the same as those in [19, Table 1 for broadband].

Frequency responses in Table 4 are plotted in Fig. 16 for Z_ms where the bandwidth for $Z_m = 73\Omega$ is the widest, 280 % (0.68-3.48 f_0). In any case, the bandwidths in Fig. 16 are all wider than that with $Z_T = 82.1\Omega$ in Fig. 14 and that for the CIT with only one TL.

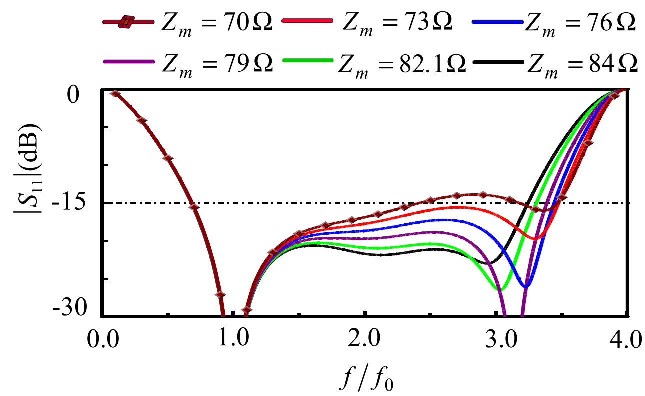

FIGURE 16. Frequency responses of CVTs in Fig. 15(b).

E. OTHER CITs

In addition to those in Fig. 7, several other CITs can be introduced by combining those in Fig. 7, converting the TLs into T-types or Π− types, or transforming the TLs into several parallel TLs. The one in Fig. 15(b) is one of them.

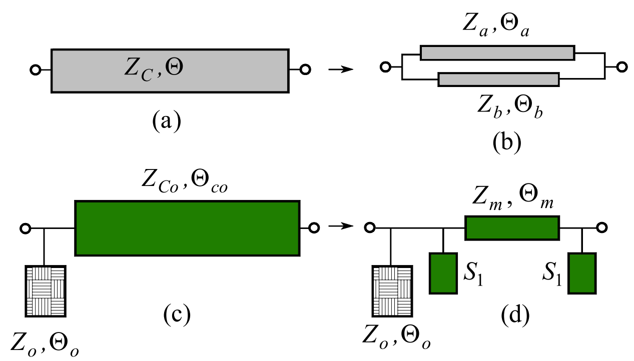

FIGURE 17. Other topologies of CITs. (a) CIT with a single TL. (b) CIT with two parallel TLs for a single TL. (C) CCTU in Fig. 7(b). (d) Converting a TL of CCTU into Π− type.

The single TL in Fig. 1 can be converted into two parallel TLs as shown in Fig. 17(a) and (b). The admittance parameters of the single TL in Fig. 17(a) are

$$[\mathbf{Y_S}] = \frac{j}{Y_C}\begin{bmatrix} -cot\Theta & \csc\Theta \\ \csc\Theta & -cot\Theta \end{bmatrix} \tag{18}$$

where $Y_C = Z_C^{-1}$. Those of the parallel TLs in Fig. 17(b) are

$$[\mathbf{Y_P}] = \frac{j}{Y_a}\begin{bmatrix} -cot\Theta_a & \csc\Theta_a \\ \csc\Theta_a & -cot\Theta_a \end{bmatrix} + \frac{j}{Y_b}\begin{bmatrix} -cot\Theta_b & \csc\Theta_b \\ \csc\Theta_b & -cot\Theta_b \end{bmatrix} \tag{19}$$

where $Y_a = Z_a^{-1}$, Θ_a, $Y_b = Z_b^{-1}$ and Θ_b are characteristic impedances and electrical lengths of the parallel TLs in Fig. 17(b). By equating (18) to (19), the design formulas for Z_b and Θ_b can be expressed as

$$Z_b^{-1} = Y_b = \sqrt{Y_C^2 + Y_a^2 + 2Y_C Y_a \left(\cot\Theta\cot\Theta_a - \csc\Theta\csc\Theta_a\right)} \tag{20a}$$

$$\cos\Theta_b = \left(\frac{Y_C\cot\Theta - Y_a\cot\Theta_a}{Y_C\csc\Theta - Y_a\csc\Theta_a}\right) \tag{20b}$$

Therefore, if the information about the single TL with Z_C and Θ is known, the implementation for the parallel TLs is possible in any case under the condition of real values of Z_b in (20).

For the CCTU in Fig. 7(b), converting the TL with Z_{Co} and Θ_{co} in Figs. 7(b) and 17(c) into a Π -type in [28, eq. (12) with $N = 1$] gives the topology in Fig. 17(d), where the two open stubs located on the left side can be combined into one open stub. The two CITs in Fig. 17(b) and (d) are the same as those in [19, Figs. 4(b) and Fig. 8(d)], respectively.

F. GUIDE LINE FOR DESIGNS

For the readers, a guide line to make use of the allowed and forbidden regions is necessary. When the two complex impedances are given, just substitute the two values into (2) and (4). If the calculation results are satisfied, no further attempt is necessary. If the calculation result of electrical length is negative, add 180° to make it positive. In this case, the electrical length of the CIT is greater than 90°. If the resulting values are thought to be long and desired to be shortened, draw three functions in (11), (13), (14) on the Smith chart to move one complex load into one of suitable regions. The cases in Sec. III. C are good examples for this.

If the calculation results of the characteristic impedances are of imaginary values, they are in the forbidden regions. To make the design possible, one complex load should be moved into one of allowed regions where the electrical lengths are less than 90°. The measured results in Fig. 11, Fig. 8 and Tables 1 and 2 are the good examples for this. If the calculated characteristic impedance is too high to realize, the good example is in Fig. 13. If the bandwidth is desired to be enlarged, the good examples are treated in Sec. III. *D*.

IV. CONCLUSIONS

In this paper, a simple and powerful design method was suggested for the CITs. The simplest circuit is only one TL, and therefore the study on the CITs with each only one TL was carried out for both complex termination impedances. However, there are restrictions such as imaginary values of characteristic impedances, too high characteristic impedances, too long electrical lengths to fabricate or small bandwidths. To solve such problems, allowed and forbidden regions were defined based on the three mapping functions which were derived for the first time in this paper, and other simple circuits adding one TL more (TL, open or short stub) were suggested. Based on CVTS in Fig. 7(a), three CITs in forbidden regions, or, imaginary values of characteristic impedances of the CITs with each only one TL, were fabricated and measured. The systematical research on the allowed and forbidden regions for both complex termination impedances may be considered as the first trial. Since the symmetric in Fig. 1 and the asymmetric CITs in Fig. 7 are basic elements, diverse applications are expected for wireless power transfer systems, power dividers with harmonic suppressions, ring hybrids and filters.

REFERENCES

[1] H.-R. Ahn, I.-S. Chang, and S.-W. Yun, “Miniaturized 3-dB ring hybrid terminated by arbitrary impedances,” *IEEE Trans. Microw. Theory Techn.*, vol. 42, no. 12, pp. 2216–2221, Dec. 1994.

[2] H.-R. Ahn, I. Wolff, and I.-S. Chang, “Arbitrary termination impedances, arbitrary power division, and small-sized ring hybrids,” *IEEE Trans. Microw. Theory Techn.*, vol. 45, no. 12, pp. 2241–2247, Dec. 1997.

[3] H.-R. Ahn and I. Wolff, “General design equations, small-sized impedance transformers, and their application to small-sized three-port 3-dB power dividers,” *IEEE Trans. Microw. Theory Techn.*, vol. 49, no. 7, pp. 1277–1288, Jul. 2001.

[4] H.-R. Ahn, *Asymmetric Passive Components in Microwave integrated Circuits*. New York, NY, USA: Wiley, 2006.

[5] H.-R. Ahn, “Modified asymmetric impedance transformers (MCCTs and MCVTs) and their application to impedance-transforming three-port 3-dB power dividers,” *IEEE Trans. Microw. Theory Techn.*, vol. 59, no. 12, pp. 3312–3321, Dec. 2011.

[6] H.-R. Ahn and S. Nam, “3-dB power dividers with equal complex termination impedances and design methods for controlling isolation circuits,” *IEEE Trans. Microw. Theory Techn.*, vol. 61, no. 11, pp. 3872–3883, Nov. 2013.

[7] J. Bito, S. Jeong, and M. M. Tentzeris, “A novel heuristic passive and active matching circuit design method for wireless power transfer to moving objects,” *IEEE Trans. Microw. Theory Techn.*, vol. 65, no. 4, pp. 1094–1101, Apr. 2017.

[8] H. R. Ahn, “Complex impedance transformers consisting of only transmission-line sections,” *IEEE Trans. Microw. Theory Techn.*, vol. 60, no. 7, pp. 2073–2084, Jul. 2012.

[9] H. Jasik, *Antenna Engineering Handbook*, 1st ed. New York, NY, USA: McGraw-Hill, 1961, ch. 31.

[10] T. A. Milligan, “Transmission-line transformation between arbitrary impedances,” *IEEE Trans. Microw. Theory Techn.*, vol. MTT-24, no. 3, p. 159, Mar. 1976.

[11] M. H. N. Potok, “Comments on ‘transmission-line transformation between arbitrary impedances,”’ *IEEE Trans. Microw. Theory Techn.*, vol. MTT-25, no. 1, p. 77, Jan. 1977.

[12] Q. He, Y. Liu, M. Su, and Y. Wu, “A compact dual-frequency transformer for frequency-dependent complex impedance load,” in *Proc. Asia Pacific Microw. Conf.*, Dec. 2012, pp. 1241–1243.

[13] Y. Liu, Y. Zhao, S. Liu, Y. Zhou, and Y. Chen, “Multi-frequency impedance transformers for frequency-dependent complex loads,” *IEEE Trans. Microw. Theory Techn.*, vol. 61, no. 9, pp. 3225–3235, Sep. 2013.

[14] O. Manoochehri, A. Asoodeh, and K. Forooraghi, “Π-model dual-band impedance transformer for unequal complex impedance loads,” *IEEE Microw. Wireless Compon. Lett.*, vol. 25, no. 4, pp. 238–240, Apr. 2015.

[15] M. A. Nikravan and Z. Atlasbaf, “T-section dual-band impedance transformer for frequency-dependent complex impedance loads,” *Electron. Lett.*, vol. 47, no. 9, pp. 551–553, Apr. 2011.

[16] M. A. Maktoomi, R. Gupta, and M. S. Hashmi, “A dual-band impedance transformer for frequency-dependent complex loads incorporating an L-type network,” in *Proc. Asia–Pacific Microw. Conf.*, vol. 1, Dec. 2015, pp. 1–3.

[17] F. Giannini and L. Scucchia, “A complete class of harmonic matching networks: Synthesis and application,” *IEEE Trans. Microw. Theory Techn.*, vol. 57, no. 3, pp. 612–619, Mar. 2009.

[18] X. Fu, D. T. Bespalko, and S. Boumaiza, “Novel dual-band matching network topology and its application for the design of dual-band class J power amplifiers,” in *IEEE MTT-S Microw. Symp. Dig.*, Montreal, QC, Canada, Jun. 2012, pp. 1–3.

[19] R. Sinha and A. De, "Theory on matching network in viewpoint of transmission phase shift," *IEEE Trans. Microw. Theory Techn.*, vol. 64, no. 6, pp. 1704–1716, Jun. 2016.

[20] R. Sinha and A. De, "Corrections to 'theory on matching network in viewpoint of transmission phase shift [Jun 16 1704-1716],"' *IEEE Trans. Microw. Theory Techn.*, vol. 65, no. 12, p. 5077, Dec. 2017.

[21] M.-L. Chuang and M.-T. Wu, "General dual-band impedance transformer with a selectable transmission zero," *IEEE Trans. Compon., Packag., Manuf. Technol.*, vol. 6, no. 7, pp. 1113–1119, Jul. 2016.

[22] P. Colantonio, F. Giannini, and L. Scucchia, "A new approach to design matching networks with distributed elements," in *Proc. 15th Int. Conf. Microw. Radar Wireless Commun.*, vol. 3, May 2004, pp. 811–814.

[23] L.-C. Tsai, "Triple-band impedance transformers using equal-length serial transmission lines," *IET Microw., Antennas. Propag.*, vol. 10, no. 5, pp. 568–573, 2016.

[24] M.-G. Chen, C.-W. Tang, T.-B. Hou, and J.-W. Wu, "Adopting the broadside coupled line for the design of an impedance transformer," in *IEEE MTT-S Microw. Symp. Dig.*, Montreal, QC, Canada, Jun. 2012, pp. 1–3.

[25] M.-G. Chen, T.-B. Hou, and C.-W. Tang, "Design of planar complex impedance transformers with the modified coupled line," *IEEE Trans. Compon., Packag., Manuf. Technol.*, vol. 2, no. 10, pp. 1704–1710, Oct. 2012.

[26] T. Jensen, V. Zhurbenko, V. Krozer, and P. Meincke, "Coupled transmission lines as impedance transformer," *IEEE Trans. Microw. Theory Techn.*, vol. 55, no. 12, pp. 2957–2965, Dec. 2007.

[27] S. Simion, "Comments on 'complex impedance transformers consisting of only transmission-line sections,"' *IEEE Trans. Microw. Theory Techn.*, vol. 61, no. 2, p. 999, Feb. 2013.

[28] H.-R. Ahn and S. Nam, "New design formulas for impedance-transforming 3-dB Marchand baluns," *IEEE Trans. Microw. Theory Techn.*, vol. 59, no. 11, pp. 2816–2823, Nov. 2011.

[29] H.-R. Ahn and S. Nam, "Compact microstrip 3-dB coupled-line ring and branch-line hybrids with new symmetric equivalent circuits," *IEEE Trans. Microw. Theory Techn.*, vol. 61, no. 3, pp. 1067–1078, Mar. 2013.

HEE-RAN AHN (S'90–M'95–SM'99) received the B.S., M.S., and Ph.D. degrees in electronic engineering from Sogang University, Seoul, South Korea.

From 1996 to 2002, she was with the Department of Electrical Engineering, Duisburg-Essen University, Duisburg, Germany, where she was involved with the Habilitation dealing with the asymmetric passive components in microwave integrated circuits. From 2003 to 2005, she was with the Department of Electrical Engineering and Computer Science, Korea Advanced Institute of Science and Technology (KAIST), Daejeon, South Korea. From 2005 to 2009, she was with the Department of Electronics and Electrical Engineering, Pohang University of Science and Technology (POSTECH), Pohang, South Korea. From 2009 to 2010, she was with the Department of Electrical Engineering, University of California, Los Angeles, CA, USA. From 2011 to 2014, she was with the School of Electrical Engineering and Computer Science, Seoul National University, Seoul, South Korea. Since 2015, she has been with the School of Electrical and Computer Engineering, Georgia Institute of Technology, Atlanta, GA, USA, as a Visiting Scholar. She authored a book entitled *Asymmetric Passive Component in Microwave Integrated Circuits* (Wiley, 2006). Her current research interests include high-frequency and microwave circuit designs, and biomedical applications using microwave theory and techniques.

MANOS M. TENTZERIS (M'98–SM'03–F'10) received the Diploma Degree *(magna cum laude)* in electrical and computer engineering from the National Technical University of Athens, Greece, and the M.S. and Ph.D. degrees in electrical engineering and computer science from the University of Michigan, Ann Arbor, MI, USA. He was a Visiting Professor with the Technical University of Munich, Germany, for the summer of 2002; a Visiting Professor with GTRI-Ireland, Athlone, Ireland, for the summer of 2009; and a Visiting Professor with LAAS-CNRS, Toulouse, France, for the summer of 2010. He is currently a Ken Byers Professor in flexible electronics with the School of ECE, Georgia Tech, Atlanta, GA, USA. He has authored over 700 papers in refereed journals and conference proceedings, five books, and 25 book chapters. He has given more than 100 invited talks to various universities and companies all over the world. He has helped develop academic programs in 3D/inkjet-printed RF electronics and modules, flexible electronics, origami and morphing electromagnetics, highly integrated/multilayer packaging for RF and wireless applications using ceramic and organic flexible materials, paper-based RFIDs and sensors, wireless sensors and biosensors, wearable electronics, "Green" electronics, energy harvesting and wireless power transfer, nanotechnology applications in RF, microwave MEMs, SOP-integrated (UWB, multiband, mmW, conformal) antennas, and heads the ATHENA Research Group (20 researchers). He has served as the Head of the GT-ECE Electromagnetics Technical Interest Group, as the Georgia Electronic Design Center Associate Director for RFID/Sensors Research, and as the Georgia Tech NSF-Packaging Research Center Associate Director of the RF Research and the RF Alliance Leader. He is a member of the URSI-Commission D, a member of the MTT-15 committee, an Associate Member of the EuMA, a Fellow of the Electromagnetic Academy, and a member of the Technical Chamber of Greece. He was a recipient/co-recipient of the 2015 IET Microwaves, Antennas and Propagation Premium Award, the 2014 Georgia Tech ECE Distinguished Faculty Achievement Award, the 2014 IEEE RFID-TA Best Student Paper Award, the 2013 IET Microwaves, Antennas and Propagation Premium Award, the 2012 FiDiPro Award in Finland, the iCMG Architecture Award of Excellence, the 2010 IEEE Antennas and Propagation Society Piergiorgio L. E. Uslenghi Letters Prize Paper Award, the 2011 International Workshop on Structural Health Monitoring Best Student Paper Award, the 2010 Georgia Tech Senior Faculty Outstanding Undergraduate Research Mentor Award, the 2009 IEEE Transactions on Components and Packaging Technologies Best Paper Award, the 2009 E.T.S.Walton Award from the Irish Science Foundation, the 2007 IEEE APS Symposium Best Student Paper Award, the 2007 IEEE IMS Third Best Student Paper Award, the 2007 ISAP 2007 Poster Presentation Award, the 2006 IEEE MTT Outstanding Young Engineer Award, the 2006 Asian-Pacific Microwave Conference Award, the 2004 IEEE Transactions on Advanced Packaging Commendable Paper Award, the 2003 NASA Godfrey "Art" Anzic Collaborative Distinguished Publication Award, the 2003 IBC International Educator of the Year Award, the 2003 IEEE CPMT Outstanding Young Engineer Award, the 2002 International Conference on Microwave and Millimeter-Wave Technology Best Paper Award (Beijing, China), the 2002 Georgia Tech-ECE Outstanding Junior Faculty Award, the 2001 ACES Conference Best Paper Award and the 2000 NSF CAREER Award, and the 1997 Best Paper Award of the International Hybrid Microelectronics and Packaging Society. He was the TPC Chair for the IEEE IMS 2008 Symposium and the Chair of the 2005 IEEE CEM-TD Workshop. He is the Vice-Chair of the RF Technical Committee (TC16) of the IEEE CPMT Society. He is the Founder and Chair of the RFID Technical Committee (TC24) of the IEEE MTT Society and the Secretary/Treasurer of the IEEE C-RFID. He is an Associate Editor of IEEE Transactions on Microwave Theory and Techniques, the IEEE Transactions on Advanced Packaging, and the *International Journal on Antennas and Propagation*. He has served as one of the IEEE MTT-S Distinguished Microwave Lecturers, from 2010 to 2012. He is one of the IEEE CRFID Distinguished Lecturers.